Materials Characterization 107 (2015) 350–357

Contents lists available at ScienceDirect

Materials Characterization

journal homepage: www.elsevier.com/locate/matchar

High-temperature creep resistance and effects on the austenite reversion and precipitation of 18 Ni (300) maraging steel

Adriano Gonçalves dos Reis [a,b,*], Danieli Aparecida Pereira Reis [a,c], Antônio Jorge Abdalla [a,d], Jorge Otubo [a,c]

[a] Instituto Tecnologico de Aeronautica – ITA, Pr. M. Eduardo Gomes, 50, São José dos Campos, SP 12228-900, Brazil
[b] Universidade Estadual Paulista - UNESP - ICT, Rodovia Presidente Dutra, km 137,8, Eugênio de Melo, São José dos Campos, SP 12247-004, Brazil
[c] Universidade Federal de São Paulo – UNIFESP, R. Talim, 330, São José dos Campos, SP 12231-280, Brazil
[d] Instituto de Estudos Avançados – IEAv, Rodovia dos Tamoios km 5,5, São José dos Campos, SP 12228-001, Brazil

ARTICLE INFO

Article history:
Received 24 April 2015
Received in revised form 30 July 2015
Accepted 1 August 2015
Available online 4 August 2015

Keywords:
Maraging 300 steel
Creep
Reverted austenite
Intermetallic precipitates

ABSTRACT

In this paper, the high-temperature creep resistance and effects on the austenite reversion and the dynamic evolution of precipitates of maraging 300 steel were investigated. The main strengthening mechanism in a solution treated and aged material is the fine needle shaped $Ni_3(Ti,Mo)$ precipitates densely dispersed in a single martensitic phase. The specimens were submitted to creep tests at temperatures of 550, 600 and 650 °C and stress conditions of 200, 300 and 500 MPa. Stress exponent (n) varied from 6.0 to 7.2 and activation energy for creep (Q_c) from 364 to 448 kJ/mol, associated to the tangled and cells arrangements of the dislocations, show that the dominant creep mechanism is controlled by dislocations climb and slip. The experimentally determined threshold stresses are about 25 MPa at 550 °C and close to 4 MPa at 600 and 650 °C. Due to high-temperature creep exposure, part of martensite was reverted to austenite in a range of 17.2% to 48.5%, depending upon the time, temperature and applied stress. At the same time, the $Ni_3(Ti,Mo)$ precipitates were coarsened and Fe_2Mo precipitated, leading to undesirable alloy's strength reduction. Volume fraction of reverted austenite showed strong negative correlation with hardness. Fracture surfaces of specimens presented ductile failure consisting of equiaxed and bi-modal dimples in the fibrous zone surrounded by 45° shear lip.

1. Introduction

The superior properties of maraging steels, such as ultra-high strength, high ductility, good hardenability, good weldability, simple heat treatment without deformation steps have led to widespread application of maraging steels for demanding applications. Hence, it has been considered to be an excellent material not only for aerospace, military and nuclear industries, but also for transportation, manufacturing, tooling, die making and electromechanical components. The high strength and high toughness comes from the precipitation strengthening of martensitic microstructure during aging heat treatment. Maraging 300 steel is a member of iron–nickel based alloy family [1–4].

Creep behavior studies on a variety of different materials and metals systems have increased significantly the understanding of the deformation mechanisms responsible for the evolution of the microstructure during plastic flow. Major improvements in creep resistance can be achieved by introducing a dispersion of fine precipitates, such as the intermetallic precipitates in maraging steels, which provide effective obstacles to dislocation movement [5]. By the other hand, the intermetallic precipitates formed during aging of maraging steels are not the stable equilibrium phases in the sense that prolonged high temperature exposure would lead to the formation of equilibrium austenite and ferrite. Since nickel, one of the major alloying elements, is an austenite stabilizer, the reversion tendency to austenite depends on whether the alloying elements enrich or deplete the matrix with respect to nickel [1–4,6]. Data available on the mechanical properties of maraging steel at elevated temperature under creep are scarce [3,7–10]. Specialized applications of the steel occasionally demand short-time exposures to high temperatures and it is desirable to have data on the creep behavior of the material during such service conditions. Although there are some research on the identification of precipitates in maraging steels [1–4,6,8,9,11–13], there is no study related to the studying of microstructure, morphology of precipitates and reverted austenite after exposure to high temperature and stress during creep tests and their relation to mechanical properties. Therefore, an investigation of microstructure and its correlation with creep behavior at high temperature in maraging 300 steel is a subject of interest and is discussed in this paper.

2. Experimental procedures

The maraging steel used in this study was a 300 grade solution treated at 820 °C — 1 h and then air cooled followed by aging at 480 °C — 3 h and then air cooled in a Brasimet Koe 40/25/65 furnace. The adopted heat treatment is the industrial practice which presents an optimal strength, ductility and toughness combination [2,3]. The chemical

* Corresponding author.
E-mail address: adriano.reis@ict.unesp.br (A.G. Reis).

http://dx.doi.org/10.1016/j.matchar.2015.08.002
1044-5803/

Table 1
Chemical composition (wt.%) of the maraging 300.

Ti	Co	Mo	Ni	Al	C	S	P	Si	Mn	Fe
0.63	9.37	4.94	19.00	0.08	0.008	0.002	0.004	0.06	0.01	Balance

composition of the material is given in Table 1. The specimens with a 18.5 mm gauge length and a 3.0 mm in diameter were submitted to constant load creep tests at temperatures of 550, 600 and 650 °C and stress conditions of 200, 300 and 500 MPa in a standard Mayes creep machine, according to ASTM E139 standard [14]. In order to characterize in terms of microstructure and mechanical properties before and after the creep tests the following tests were performed: dilatometry (Linseis model L75V 1400 RT), microhardness (FutureTech model FM-700), X-ray diffraction (Panalytical model X'Pert Powder), optical microscopy (Carl Zeiss model Axio Imager 2), scanning electron microscopy (TESCAN model VEGA 3) and transmission electron microscopy/energy dispersive X-ray micro-analysis (Philips TECNAI model G2F20 TEM).

3. Results and discussion

3.1. Characteristic of the material before creep tests

Table 2 shows transformations temperatures obtained from dilatometry test for the maraging 300 and represented as P_s (Precipitation start), P_f (Precipitation finish), A_s (Austenite formation start), A_f (Austenite formation finish), M_s (Martensite formation start) and M_f (Martensite formation finish). The results indicate that the material should have a single martensitic phase structure upon cooling to room temperature as far as the M_f is 62 °C.

The X-ray diffraction (XRD) pattern in the 2θ ranging from 35–105° is shown in Fig. 1. The XRD spectra confirm that the microstructure of the solution treated and aged specimen is completely martensitic at room temperature corroborating with dilatometry result. The light micrograph shown in Fig. 2 indicates that the microstructure consists essentially of lath martensite. Transmission electron microscopy of the sample is shown in Fig. 3. The bright-field (BF) micrograph, Fig. 3a, shows the basic microstructure comprising of aligned laths martensite. The Fig. 3b shows the BF image of tangled dislocations within lath martensites and densely dispersed and very fine needle shaped Ni_3(Ti,Mo) precipitates. Dislocation density for solution treated and aged sample is of the order of 10^{10} mm^{-2}. Higher magnification in Fig. 3c shows the BF image of Ni_3(Ti,Mo) precipitates with average diameter of 1.6 nm and average length of 13 nm. Fig. 3d is the corresponding SAD pattern using the $[1\bar{1}3]$ zone axis and specific spots. Table 3 shows the chemical composition by EDS/TEM of matrix and Ni_3(Ti,Mo) precipitate showing that the precipitate is rich in Mo, Ti and Ni. Ni_3(Ti,Mo) precipitates at this aging temperature are the main strengthening phase since they are coherent with the martensitic matrix and provide effective resistance to the motion of dislocation during deformation. The average hardness increased from 331 ± 5 HV in the solution treated condition to 604 ± 18 HV after aging. The precipitation behavior and precipitation hardening mechanism at the aging temperature in this study are supported by other reports [2,4,6,8,9,11–13].

Table 2
Transformation temperatures of the maraging 300 steel.

	P_s	P_f	A_s	A_f	M_s	M_f
Temperature (°C)	500	595	623	801	194	62

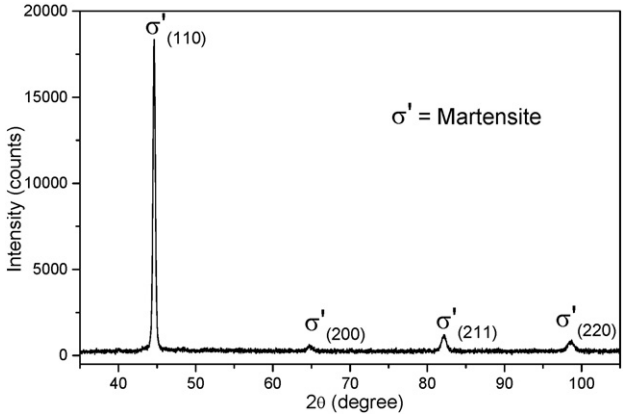

Fig. 1. XRD pattern for the solution treated and aged maraging 300 showing peaks corresponding to the martensite phase.

3.2. Creep behavior

Fig. 4 displays a representative creep curve of strain rate ($d\varepsilon/dt$) versus strain (ε) at 600 °C and 300 MPa. Maraging 300 steel exhibits typical creep curves consisting of well-defined primary (I), secondary (II) and, when submitted to the rupture, the tertiary (III) stage. A relatively short initial period in which the primary creep rate decreases is probably associated with hardening due to the accumulation of dislocations. However, most of the creep life is dominated by a constant creep rate that is thought to be associated with a stable dislocation configuration due to the recovery and hardening process [5]. The results from creep tests are summarized in Table 4, which shows the values of the secondary creep rate ($\dot{\varepsilon}_s$) and, when submitted to the rupture, the time to rupture (t_r), the percent elongation (EL) and percent reduction in area (RA). From the Table 4, it is possible to notice that $\dot{\varepsilon}_s$ increase as the temperature or stress increase and t_r presents reverse behavior accordingly. At 650 °C the increase of secondary creep rate is more pronounced since this temperature is higher than A_s.

For most metal and alloys, the relationship between the strain rate ($\dot{\varepsilon}_s$), stress (σ) and temperature (T) can be expressed by the power-law creep equation:

$$\dot{\varepsilon}_s = A\sigma^n exp(-Q_c/RT) \quad (1)$$

where Q_c is the activation energy for creep, A is a constant that depends on the microstructure, temperature and applied stress (σ), n is the

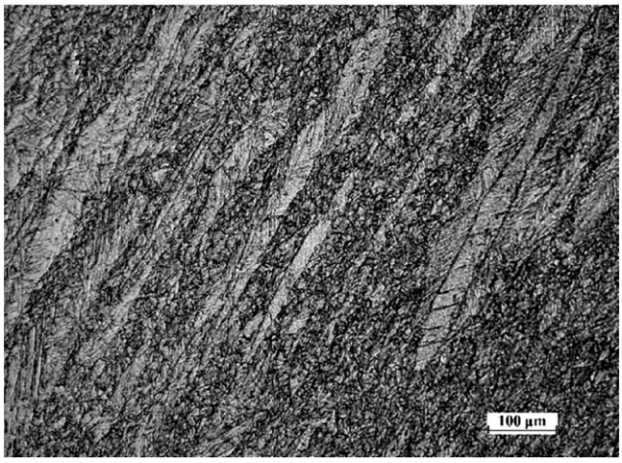

Fig. 2. Optical micrograph of the solution treated and aged maraging 300 showing lath martensites.

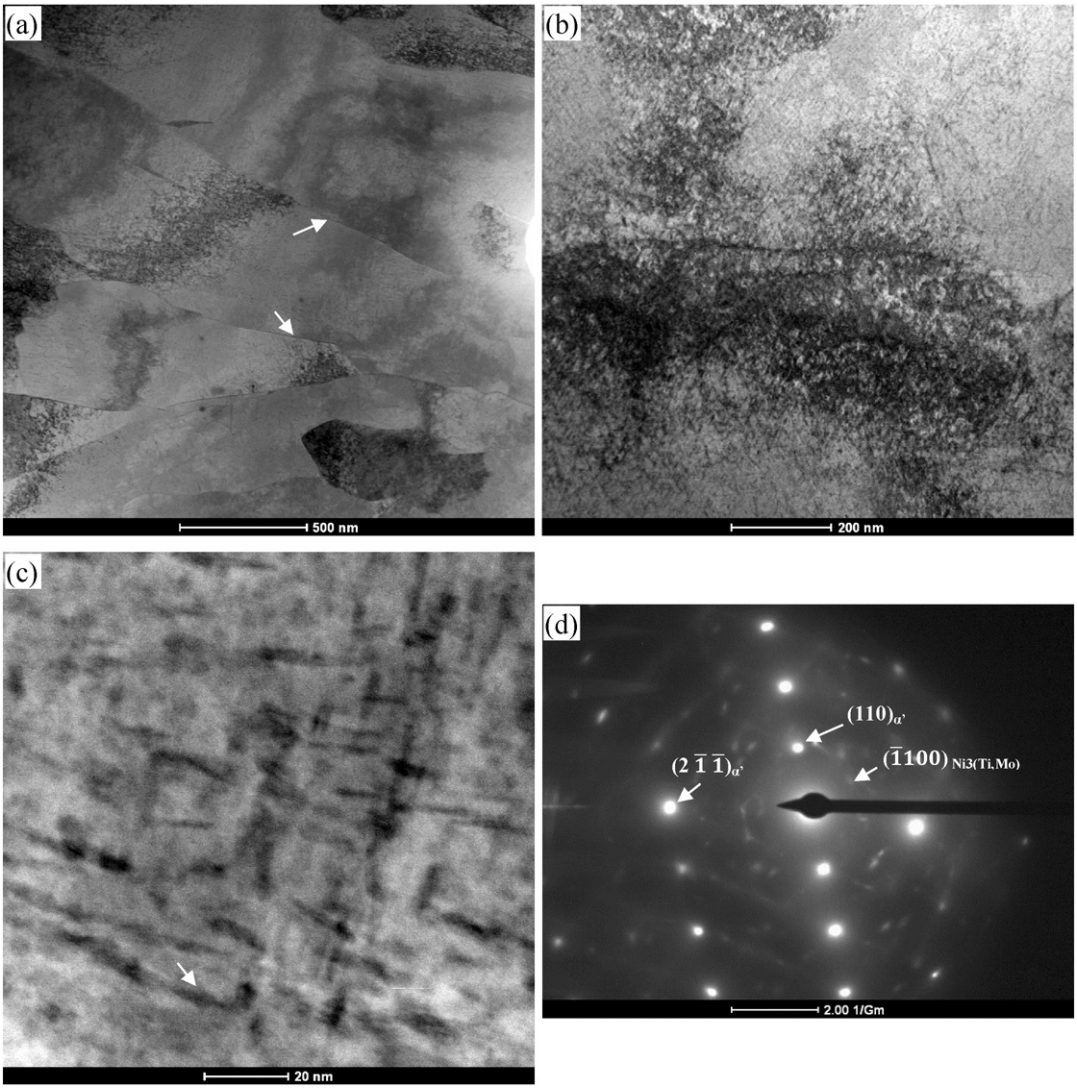

Fig. 3. TEM micrographs of the solution treated and aged maraging 300 showing (a) aligned lath martensites, (b) tangled dislocations and very finely dispersed needle shaped Ni3(Ti,Mo) precipitates, (c) details of needle shaped Ni3(Ti,Mo) precipitates and (d) corresponding SAD pattern using the [1$\bar{1}$3] zone axis and specific spots of needle shaped Ni3(Ti,Mo) precipitate.

stress exponent, R is the universal gas constant and T absolute temperature. The combination of Q_c and n values indicates the main creep mechanism that controls a given deformation process [5]. The slopes of the plot $ln\dot{\varepsilon}_s x\ ln\sigma$, which is presented in Fig. 5, provide an estimate of n. The slopes of the plot $ln\dot{\varepsilon}_s x\ ln1/T$, which is presented in Fig. 6, provide an estimate of Q_c.

The values of n between 6.0 and 7.2 and Q_c between 364 kJ/mol and 448 kJ/mol are in accordance with results reported in the literature to materials hardened by a dispersion of a second-phase particles that are considerable greater than the values expected for the appropriate base materials (iron: $n = 5$ and $Q_c = 284$ kJ/mol). The expected stress exponent values for these materials are in the range of 5 to 15 [5,15]. Furthermore, Viswanathan et al. [7] who used indentation technique for evaluating high temperature creep of maraging 350 steel, obtained Q_c values between 405 kJ/mol and 467 kJ/mol.

Table 3
Chemical composition (wt.%) by EDS/TEM of maraging 300 steel after solution treated and aged condition.

Elements	Ti	Co	Mo	Ni	Fe
Matrix	0.452	9.423	1.344	12.456	76.325
Ni_3(Ti,Mo)	4.118	8.360	10.496	18.985	58.041

The Eq. (1) is used to interpret the creep behavior of pure metals and solid solution alloys. However, the use of this equation for particle hardened metals and alloys often gives rise to extremely high values of stress

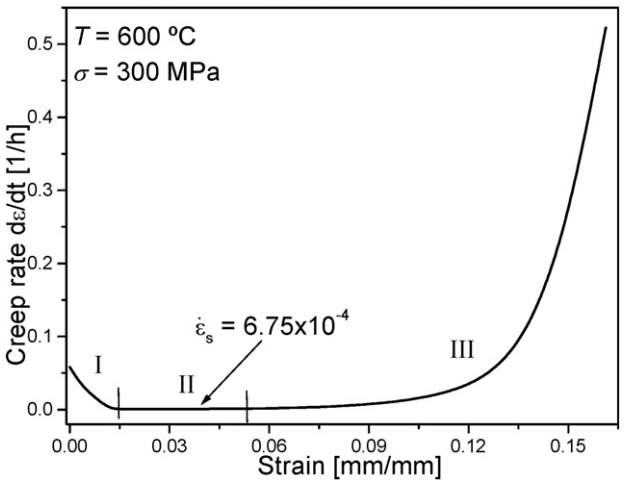

Fig. 4. Creep strain rate dε/dt versus strain of maraging 300 at 600 °C and 300 MPa.

Table 4
Creep data at 550 °C, 600 °C and 650 °C.

Temperature (°C)	σ (MPa)	$\dot{\varepsilon}_s$ (1/h)	t_r (h)	EL (%)	RA (%)
550	200	4.49×10^{-6}	[a]	–	–
	300	1.51×10^{-5}	[a]	–	–
	500	9.98×10^{-4}	56.00	23.2	67.4
600	200	4.89×10^{-5}	[a]	–	–
	300	6.75×10^{-4}	77.90	22.6	64.0
	500	3.44×10^{-2}	1.50	21.4	70.6
650	200	2.07×10^{-3}	29.35	28.4	69.0
	300	2.87×10^{-2}	2.00	36.7	69.3
	500	1.34	0.05	25.0	72.0

[a] Interrupted tests before rupture.

exponent ($n>>5$) as well as activation energy for creep appears relatively high (greater than lattice self-diffusion of the matrix). It is a standard procedure in these materials to interpret the deformation in terms of an effective stress, σ_e, which is defined as $(\sigma - \sigma_0)$ where σ_0 is a threshold stress delineating a lower limiting stress for any measurable flow [16,17]. Under these conditions, Eq. (1) could be replaced by:

$$\dot{\varepsilon}_s = A(\sigma - \sigma_0)^n exp(-Q_c/RT). \quad (2)$$

The values of σ_0 are then estimated either by plotting $\dot{\varepsilon}^{1/n}$ as a function of σ on linear axes for selected values of n and extrapolating linearly to zero creep rate [16,17] or by directly extrapolating the creep data to very low strain rates [18]. Although the stress exponents n shown in Fig. 5 are reasonably low, it is possible also to interpret the data using Eq. (2). Considering the narrow strain rate interval examined in this work, the σ_0 is estimated by plotting $\dot{\varepsilon}^{1/n}$ as a function of σ according to Fig. 7, which shows that the σ_0 are, respectively, close to 4 MPa at 600 °C and 650 °C and close to 25 MPa at 550 °C. Threshold stresses have been estimated from tests conducted on a number of particle hardened metals and alloys and the results reveal that the values of σ_0 generally decrease with increasing the test temperature and also takes into account the precipitates size [16,17].

The correlation between activation energy (Q_c) and the stress exponent from secondary creep (n) shown in Figs. 5 and 6 suggests that the mechanism of creep on the secondary stage is controlled by dislocation climb [5,15]. Although creep mechanism prediction was estimated based on parameters obtained in creep curves, it is important to verify those assertions through microstructural examination. TEM was used to study the fine structural details in the specimens to observe the different microstructural features left after the creep test. Fig. 8 shows a

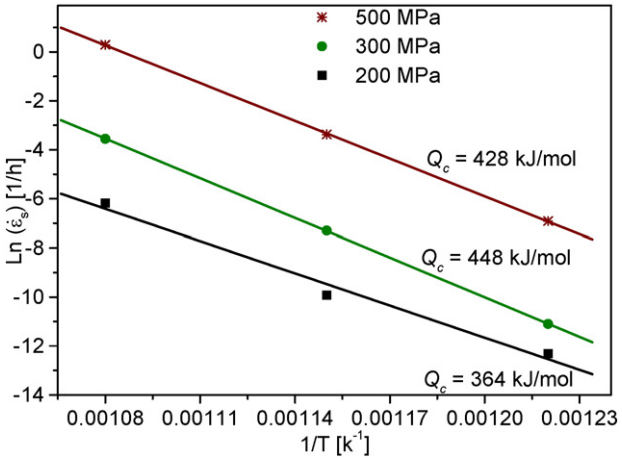

Fig. 6. Dependence of steady-state rate on temperature for maraging 300 at 200 MPa, 300 MPa and 500 MPa (the slope is $-Q_c/R$).

representative bright-field TEM image of the sample after the creep test at 600 °C and 500 MPa. What was originally fairly uniform dislocation configuration (Fig. 3b), after the creep test it is converted into very heterogeneous structure, with some areas with high density of dislocation tangles and networks, whereas some others which are relatively dislocation free. It can be noticed also that the dislocation density in the matrix decreases owing to the high temperature due to fast recovery. However, quantification of dislocation density after creep exposure is not appropriate due to the not uniform dislocation distribution in the matrix and the high volume fraction of reverted austenite and precipitation coarsening that could result in an imprecise result. This microstructural features was evidenced in all conditions of stress and temperature analyzed. TEM studies on the specimens revealed the presence of dislocation arrangements as was expected by creep parameters and suggests the dislocation mechanism of creep.

3.3. Characteristic of the samples after the creep tests

In alloys such as maraging 300 steel, the precipitation usually continues in service during creep, and equilibrium phases are attained after extended times [5]. Reversion of martensite to austenite in the temperature range of 550 °C to 650 °C produces different amount of reverted austenite [2,19]. Fig. 9 shows the representative light micrograph of the sample after creep test at 650 °C and 500 MPa. The austenite reversion is clearly shown in this microstructure. The bright patchy regions, indicated by arrows in the micrograph, correspond to regions

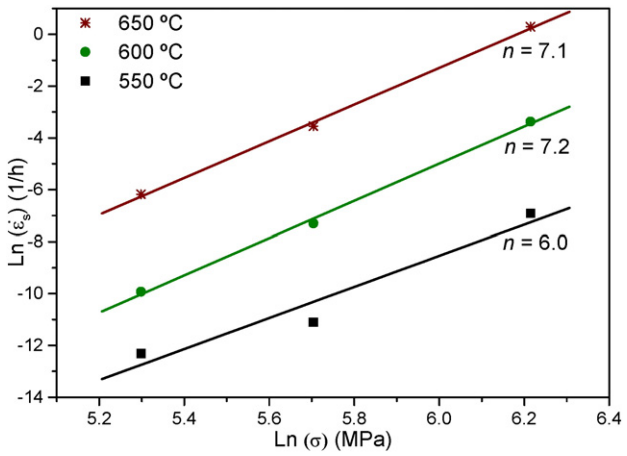

Fig. 5. Dependence of steady-state rate on applied stress for the maraging 300 at 550 °C, 600 °C and 650 °C (the slope is n).

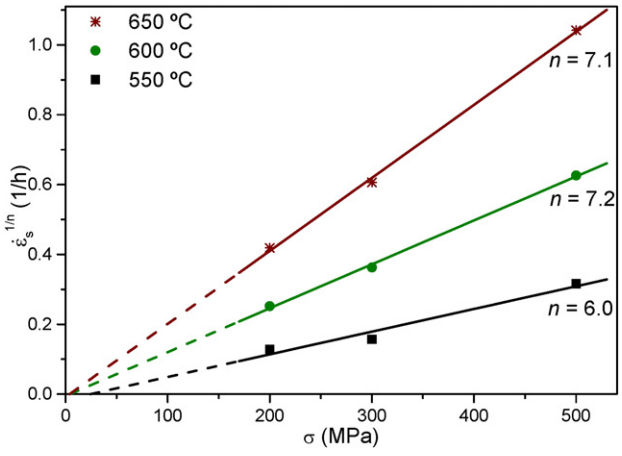

Fig. 7. $\dot{\varepsilon}^{1/n}$ as a function of σ plot for determination of threshold stress, σ_0, in maraging 300 steel at 550 °C, 600 °C and 650 °C by back extrapolation (dash line).

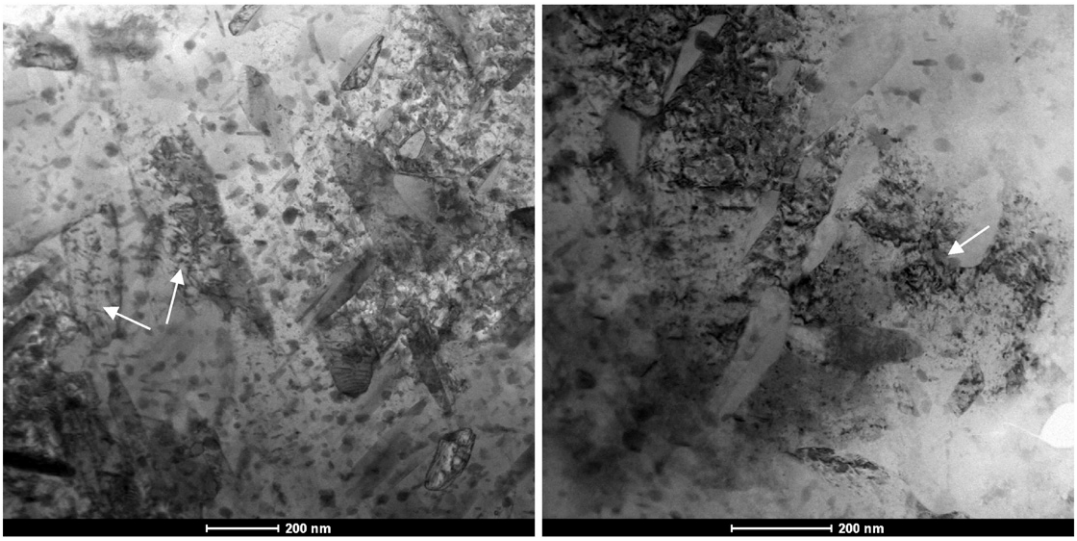

Fig. 8. TEM bright field micrographs of maraging 300 crept at 600 °C and 500 MPa showing heterogeneous dislocation structure.

having considerable reverted austenite fraction. Optical microscopy is very useful to show morphology and distribution of the reverted austenite. However, quantification using this technique is not appropriated since the reverted austenite of maraging steels presents very fine microstructure and it is not uniformly distributed, as shown in Fig. 9.

Volume fraction of austenite can be estimated from the α'_{110} and γ_{111} peaks of martensite and austenite, respectively, as per the direct comparison method [20]. Fig. 10 displays a representative X-ray diffraction patterns in the 2θ range 42–46° after creep test at 650 °C and stresses of 200, 300 and 500 MPa, where it can be seen the intense peaks of γ_{111} of austenite phase. Table 5 summarizes the volume fractions of reverted austenite for a set of the temperatures and stresses tested where it is possible to notice that the volume fraction of austenite increased with increasing temperature and/or time. At 650 °C the volume fraction of austenite is more pronounced since this temperature is higher than A_s (Table 2). Even in temperatures of 550 °C and 600 °C, which are lower than A_s, an expressive amount of reverted austenite is observed. Austenite reversion in maraging steels cannot be eliminated entirely when these alloys are reheated to temperatures below the A_s for prolonged periods, because the martensite that is formed during solution treatment is metastable and the system decomposes to the equilibrium austenite and ferrite structures via diffusion-controlled reactions.

Fig. 11 shows representative TEM images of the sample crept at 600 °C and 500 MPa. Fig. 11a shows an overview of the precipitates and reverted austenite distribution in the matrix. A great amount of reverted austenite forms inside the lath and along the lath martensite boundaries, which matches the fraction of 25.8% of reverted austenite by X-ray result. Fig. 11b is a higher magnification image showing that the precipitates coarsening is obvious with large interparticle spacing compared to just aged samples. Fig. 11c is a higher magnification image showing the precipitates morphology. The size of $Ni_3(Ti,Mo)$ precipitates are larger than those before creep tests, showing an average diameter of 8 nm and average length of 68 nm. After creep test, globular Fe_2Mo precipitates are also revealed and they are distributed in the matrix with an average diameter of 32 nm. $Ni_3(Ti,Mo)$ and Fe_2Mo precipitates are confirmed by SAD pattern and specific spots according Fig. 11d and the reverted austenite is also confirmed by SAD pattern according Fig. 11e.

Table 6 shows the chemical composition of matrix, precipitates and reverted austenite by EDS/TEM of the sample crept at 600 °C and 500 MPa. Corroborating with SAD pattern (Fig. 11), Table 6 shows that $Ni_3(Ti,Mo)$ precipitate is rich in Mo and Ti and Fe_2Mo precipitate is

Fig. 9. Optical micrograph of maraging 300 crept at 650 °C and 500 MPa showing bright regions of reverted austenite.

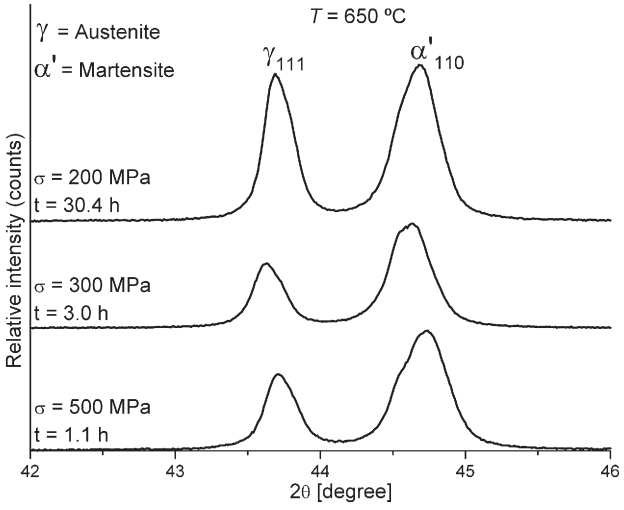

Fig. 10. XRD pattern for the maraging 300 crept at 650 °C varying stresses (σ) and time (t) showing peaks corresponding to the martensite and austenite phases.

Table 5
Volume fraction of reverted austenite phase of the samples after creep tests at 550 °C, 600 °C and 650 °C.

Temperature (°C)	σ (MPa)	Time of creep exposure (h)	Austenite volume fraction (%)
550	200	363.0[a]	18.6
	300	966.4[a]	21.8
	500	57.0	17.2
600	200	385.0[a]	29.0
	300	78.9	27.4
	500	2.5	25.8
650	200	30.4	48.5
	300	3.0	38.9
	500	1.1	38.3

[a] Interrupted tests before rupture.

Table 6
Chemical composition (wt.%) by EDS/TEM of maraging 300 steel crept at 600 °C and 500 MPa.

Elements	Ti	Co	Mo	Ni	Fe
Matrix	0.357	9.713	1.005	11.544	77.381
Austenite	0.140	6.452	7.365	30.723	55.320
$Ni_3(Ti,Mo)$	4.510	8.165	10.998	18.783	57.544
Fe_2Mo	Undetectable	6.882	26.610	10.143	56.365

rich in Fe and Mo. The reverted austenite, as expected, is rich in Ni, beside the matrix showed an expressive depletion in Ni. The formation mechanism of reverted austenite in maraging steels is supposed to be a diffusion-controlled process. It was assumed that the formation of reverted austenite is connected to the dissolution of the metastable Ni_3Mo precipitates, at high creep test temperatures such as 600 °C, promoting the Ni enrichment of the matrix, and this enrichment is further enhanced due to iron depletion as the Fe_2Mo phase nucleates and grows. Since the austenite is enriched with the austenite stabilizing element nickel, it does not transform to martensite on cooling to room temperature [1,2,4,11,21,22].

Particle coarsening increases both the average particle size and the mean interparticle spacing, so the creep resistance decreases gradually with time, as fewer particles are present to hinder the dislocation movement [5]. The precipitates coarsening and loss of coherence between precipitates and martensitic matrix result in a hardness drop, although the reverted austenite has a larger degree of influence on hardness and strength over the coarsening of precipitates. Fig. 12 shows the strong negative correlation between volume fraction of austenite and

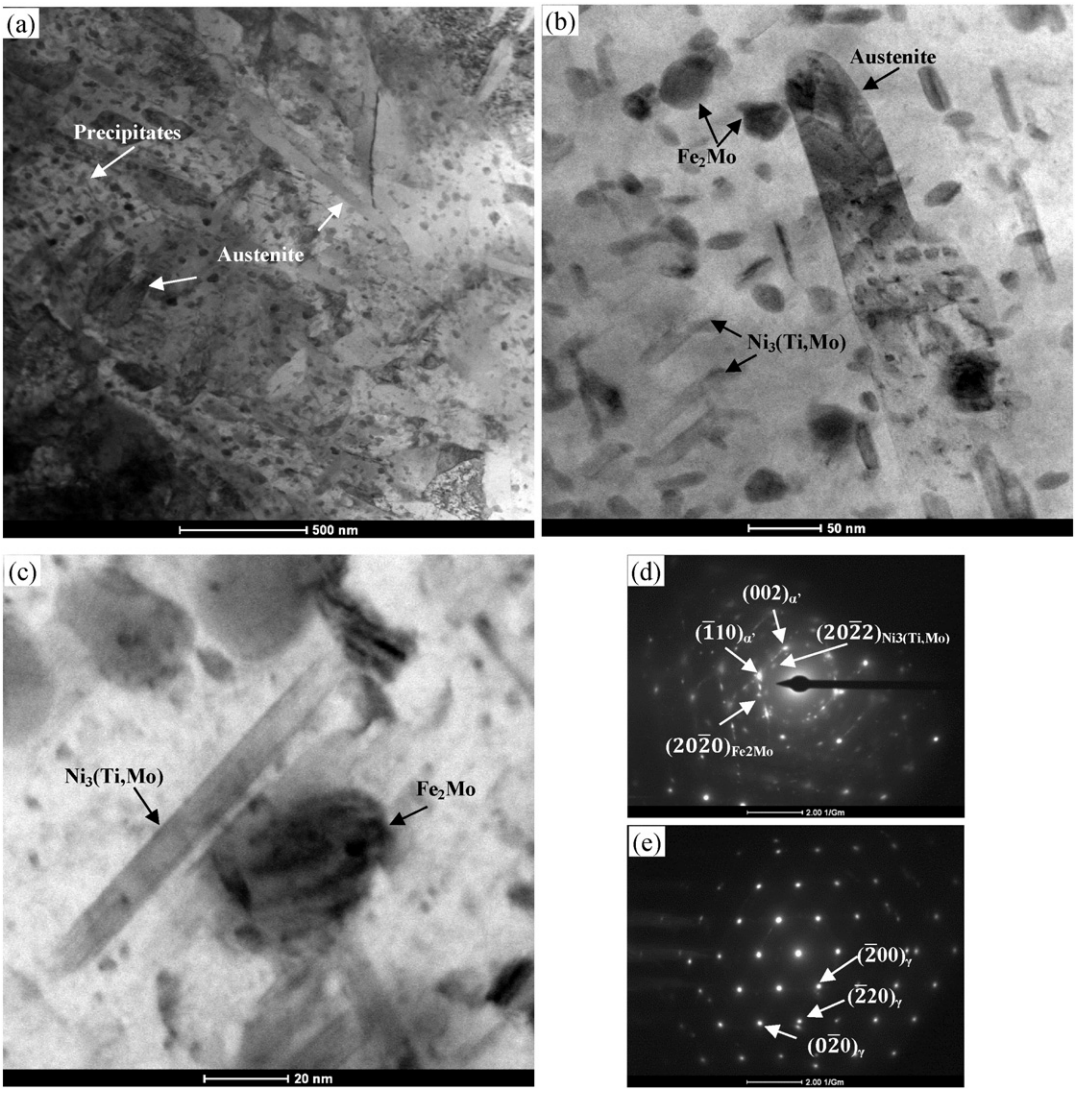

Fig. 11. TEM micrographs of maraging 300 crept at 600 °C and 500 MPa showing (a) precipitates and reverted austenite distribution in the matrix, (b) $Ni_3(Ti,Mo)$ and Fe_2Mo precipitates and reverted austenite, (c) needle shaped $Ni_3(Ti,Mo)$ precipitate and globular Fe_2Mo intermetallic precipitates morphology, and corresponding SAD pattern and specific spots of (d) $Ni_3(Ti,Mo)$ and Fe_2Mo and (e) reverted austenite.

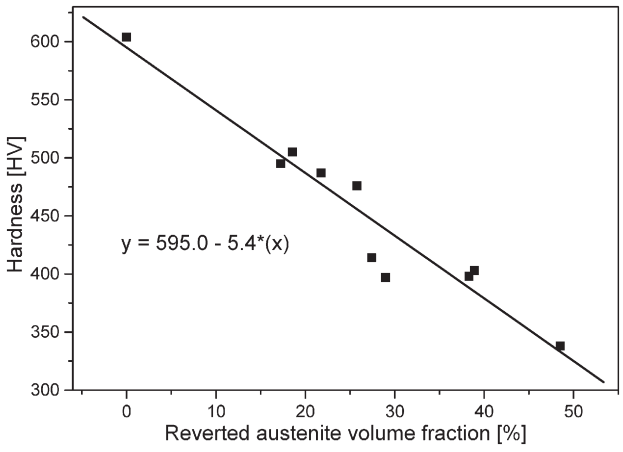

Fig. 12. Correlation between volume fraction of reverted austenite and hardness of maraging 300 before and after creep tests at 550 °C, 600 °C and 650 °C.

hardness, where it can be noticed that the increase of the volume fraction of the reverted austenite produces a substantial drop in the hardness for the crept samples at 550, 600 and 650 °C in different time and stress conditions. Minimum hardness value is obtained in the sample crept at 650 °C for 30.4 h, achieving a hardness value of 338 HV close to the value found in the solution treated sample.

3.4. Characteristics of fracture surfaces

Fracture surfaces of specimens after creep tests showed a cup-and-cone fracture morphology, characteristic of a ductile failure. Fig. 13a is a SEM micrograph showing an overview of the fracture surface consisting of dimpled rupture in the fibrous zone surrounded by 45° shear lip, with a gross permanent or plastic deformation in the region of ductile fracture. Fig. 13b is a higher magnification image of the 45° shear lip at the location enclosed in Fig. 13a showing the elongated C-shaped dimples due to tensile shearing near the end of the fracture, opposite to the origin. Fig. 13c is a higher magnification image of the equiaxed dimples at the location enclosed in Fig. 13a, which shows a

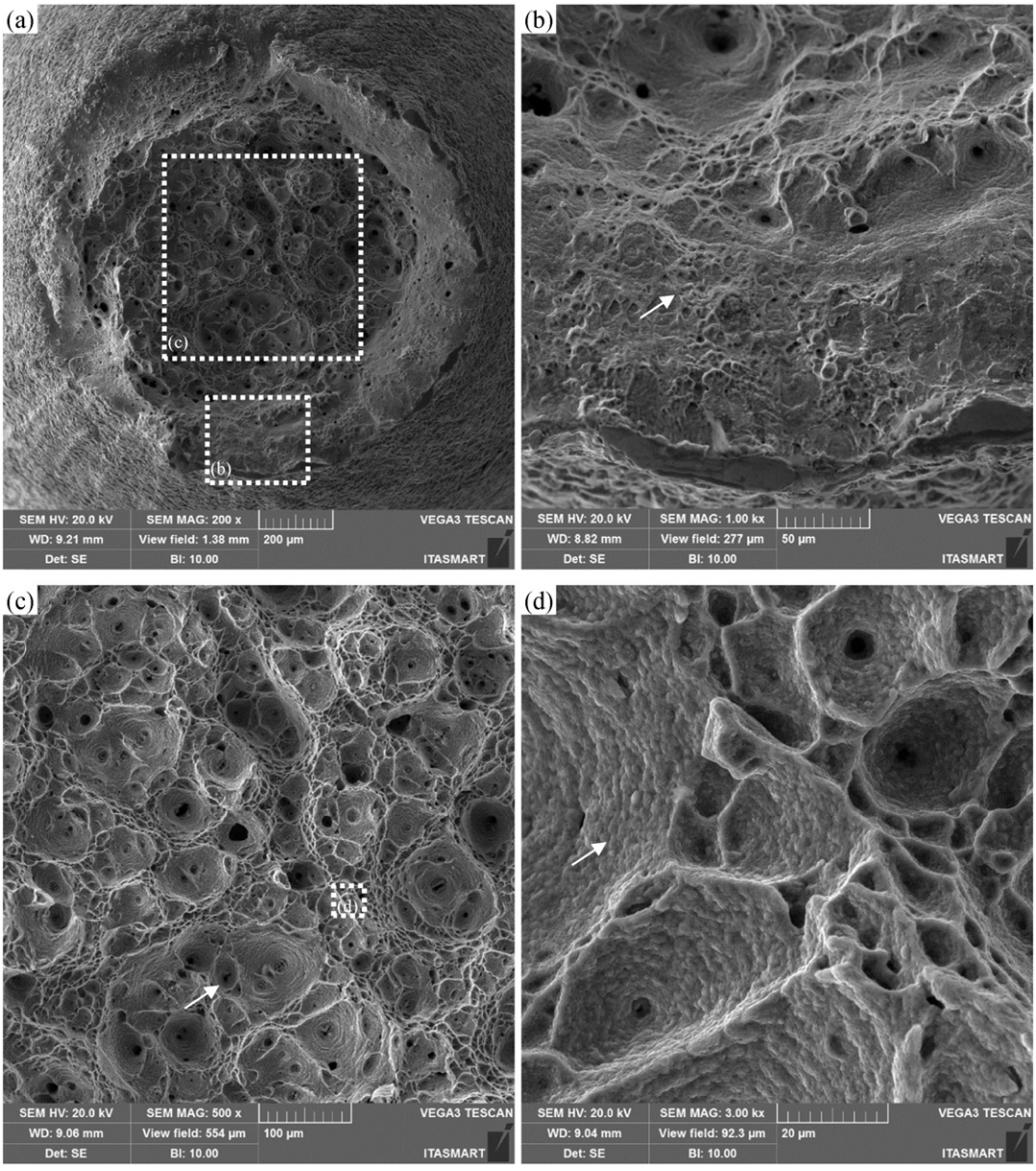

Fig. 13. SEM micrographs of maraging 300 crept at 650 °C and 500 MPa showing fracture surfaces: (a) typical cup-and-cone, (b) 45° shear lips with C-shaped dimples, (c) equiaxed dimples and (d) slip lines.

bi-modal structure with small change in depth. Fig. 13d is a higher magnification image of the equiaxed dimples at the location enclosed in Fig. 13c showing the slip lines and corrugated surfaces. The size and shape of dimples are driven by the number and distribution of nucleated microcavities and by the internal stress level.

4. Conclusions

The following conclusions are drawn based on the present work on maraging 300 steel:

- The main strengthening mechanism of the solution treated and aged sample is the fine needle shaped Ni_3(Ti,Mo) precipitates densely dispersed in a single martensitic phase;
- Typical creep curves consisting of well-defined primary, secondary and, when submitted up to the rupture, the tertiary stages were found. Based on the stress exponent (n), activation energy for creep (Q_c) and heterogeneous dislocation structure, it is concluded that the dominant creep mechanism is primarily controlled by dislocation climb and slip. A threshold stress is present mainly at 550 °C;
- During creep tests, part of martensite was reverted to austenite and concomitantly the Ni_3(Ti,Mo) precipitates coarsened and Fe_2Mo precipitated leading to undesirable strength reduction. Volume fraction of austenite showed a strong negative correlation with hardness;
- Dominant type of failure was ductile showing a typical cup-and-cone fracture morphology, consisting of equiaxed and bi-modal dimples in the fibrous zone surrounded by 45° shear lip.

Acknowledgments

The authors are grateful to CNPq (grants 141274/2013-1 and 475194/2011-0) and CAPES (Proj. Pro-Defesa 014/08) for the financial support.

References

[1] E. Pereloma, D.V. Edmonds, Phase Transformations in Steels: Diffusionless Transformations, High Strength Steels, Modelling and Advanced Analytical Techniques, Woodhead Publishing Limited, New Delhi, 2012.
[2] W. Sha, Z. Guo, Maraging Steels: Modelling of Microstructure, Properties and Applications, Woodhead Publishing Limited, Boca Raton, 2009.
[3] A.M. Hall, C.J. Slunder, The Metallurgy, Behavior, and Application of the 18-Percent Nickel Maraging Steels: A Survey, NASA — Battelle Memorial Institute, Washington, D.C., 1968 (NASA SP-5051).
[4] M. Schmidt, K. Rohrback, Heat treating of maraging steels, ASM Handbook Committee. ASM Handbook: Heat Treating, tenth edASM International, Materials Park 1991, pp. 528–548 (v. 4).
[5] R.W. Evans, B. Wilshire, Introduction to Creep, The Institute of Materials, London, 1993.
[6] U.K. Viswanathan, G.K. Dey, V. Sethumadhavan, Effects of austenite reversion during overageing on the mechanical properties of 18 Ni (350) maraging steel, Mater. Sci. Eng. A 398 (2005) 367–372.
[7] U.K. Viswanathan, T.R.G. Kutty, R. Keswani, C. Ganguly, Evaluation of hot hardness and creep of a 350 grade commercial maraging steel, J. Mater. Sci. 31 (1996) 2705–2709.
[8] G. Gurewitz, N. Atzmon, A. Rosen, Creep and stress relaxation in 18% Ni (250) maraging steel, Met. Technol. 4 (1977) 62–65.
[9] J.E. Campbell, F.J. Barone, D.P. Moon, The Mechanical Properties of the 18 Per Cent Nickel Maraging Steels, Columbus: Defense Metals Information Center - Battelle Memorial Institute, DMIC Report 1981964.
[10] A.G. Reis, D.A.P. Reis, A.J. Abdalla, J. Otubo, Effect of plasma nitriding on creep behavior at 550 °C of a maraging steel (300 grade) solution annealed, Mater. Sci. Forum 802 (2014) 452–456.
[11] F. Zhu, Y.F. Yin, R.G. Faulkner, Microstructural control of maraging steel C300, Mater. Sci. Technol. 27 (2011) 395–405.
[12] V.K. Vasudevan, S.J. Kim, C.M. Wayman, Precipitation reactions and strengthening behavior in 18 Wt Pct nickel maraging steels, Metall. Trans. A 21A (1990) 2655–2668.
[13] I. Tewari, S. Mazumder, I.S. Batra, G.K. Dey, S. Banerjee, Precipitation in 18 wt% Ni maraging steel of grade 350, Acta Metall. 48 (2000) 1187–1200.
[14] American Society for Testing and Materials, ASTM E139-11: Standard Practice for Conducting Creep, Creep–Rupture and Stress–Rupture Tests of Metallic Materials, 2011 (Philadelphia).
[15] J. Bressers, Creep and Fatigue in High Temperature Alloys, Applied Science Publishers, London, 1981 (190 pp.).
[16] T.G. Langdon, Dislocations and creep, Conference to Celebrate the Fiftieth Anniversary of the Concept of Dislocation in Crystals, 11–12. Dec. 1984. London. Proceeding, The Institute of Metals, London 1985, pp. 221–237.
[17] M.E. Kassner, M.T. Pérez-Prado, Fundamentals of Creep in Metals and Alloys, first edition Elsevier, Kidlington, 2004 (288 pp.).
[18] J.C. Gibeling, W.D. Nix, The description of elevated temperature deformation in terms of threshold stresses and back stresses: a review, Mater. Sci. Eng. 45 (1980) 123–135.
[19] J.M. Pardal, S.S.M. Tavares, M.P. Cindra Fonseca, Study of the austenite quantification by X-ray diffraction in the 18Ni–Co–Mo–Ti maraging 300 steel, J. Mater. Sci. 41 (2006) 2301–2307.
[20] B.D. Cullity, S.R. Stock, Elements of X-Ray Diffraction Third Ed, Prentice-Hall, New Jersey, 2001.
[21] M. Farooque, H. Ayub, A. Ul Haq, A.Q. Khan, The formation of reverted austenite in 18% Ni 350 grade maraging steel, J. Mater. Sci. 33 (1998) 2927–2930.
[22] X. Li, Z. YIN, Reverted austenite during aging in 18Ni(350) maraging steel, Mater. Lett. 24 (1995) 239–242.